

Numerical Study of Interfacial Problems with Small Surface Tension

Hector D. Ceniceros and Thomas Y. Hou

ABSTRACT. This paper reviews some recent advances in developing stable and efficient boundary integral methods for solving interfacial flows with surface tension. Both spatial and temporal stability issues are discussed in detail. We then use these highly accurate and stable methods to investigate the peculiar regularization effect of small surface tension in overturning water waves, unstably stratified two-fluid interfaces, and Hele-Shaw flows. Several interesting and surprising phenomena are revealed in the limit of small surface tension. This paper is not intended to be a general survey of the subject and the discussion is limited by both the taste and expertise of the authors.

1. Introduction

Surface tension plays a fundamental role in the development of several important physical phenomena. Examples vary from materials science and engineering applications such as pattern formation in crystal growth and dendritic solidification to nonlinear phenomena in fluids such as capillary waves, droplet formation, fingering instabilities in porous media, and the appearance of finite-time singularities to name only a few.

Surface tension at an interface between two immiscible fluids arises from the imbalance of their intermolecular cohesive forces. It is thus, an ever-present force although it could be very small. But even very small surface tension can have dramatic effects on the nonlinear evolution of a fluid or material (as in the case of crystal growth) interface. The numerical study of small surface tension has both physical and mathematical implications. On the physical stand, it contributes to the understanding of important observable phenomena. On the mathematical stand, it provides valuable information about the structure and behavior of the solutions, and about the dependence of the solutions on the small parameter. Last but not least, the knowledge of the limiting behavior of the interface solutions as surface tension tends to zero, constitutes a critical test to the validity of the simplified zero-surface-tension modeling equations. This has a profound implication. Neglecting seemingly small terms can lead to an unphysical model.

1991 *Mathematics Subject Classification.* Primary 65M12, 76B15.

Research supported in part by a NSF Grant DMS-9704976 and by an ARO Grant DAAD19-99-1-0141.

Numerically, one can approach the investigation of interfacial evolution with small surface tension with different techniques. For example, phase field models, volume-of-fluid methods, level set methods, front tracking, and boundary integral/element methods. Boundary integral methods outperform other numerical methods when it comes to the accurate resolution of the small scale and often very singular structures characteristic of surface tension effects. Our discussion here focuses exclusively on boundary integral methods.

One of the advantages of using boundary integral methods is that it reduces the two dimensional problem into a one dimensional problem involving quantities along the interface only. Consequently, their use avoids the difficulty of differentiating discontinuous fluid quantities across the fluid interface. However, numerical simulations using boundary integral methods also suffer from the sensitivity to numerical instabilities because the underlying problems are very singular [LHC76, Rob83, Do192]. Straight-forward discretizations may lead to numerical instabilities. It turns out that a certain *compatibility* is required between the choice of the quadrature rule for the singular velocity integral and the choice of the spatial derivative. This compatibility ensures that a delicate balance of terms that holds on the continuous level is preserved on the discrete level. This balance is crucial for maintaining numerical stability. A stability analysis by Beale, Hou, and Lowengrub [BHL96] for a boundary integral method for two-dimensional water waves reveals that certain Fourier filtering is needed to maintain the compatibility condition at the discrete level. With this filtering, determined by the choices of the quadrature rule and of the approximation for the spatial derivative, one can prove stability of the boundary integral method for water waves [BHL96] and for multi-fluid interfaces if surface tension is included [CH98].

While the spatial discretizations are proved to be stable and convergent, stability of the time discretization is very difficult to obtain in the presence of surface tension. Surface tension introduces a large number of spatial derivatives through the local curvature. If an explicit time integration method is used, these high order derivative terms induce strong stability constraints on the time step. For example, the time step stability constraint for the Hele-Shaw flows is given by $\Delta t \leq Ch^3$, where Δt is the time step, and h is the minimum particle spacing. These stability constraints are time dependent and become more severe by the differential clustering of points along the interface.

Hou, Lowengrub, and Shelley [HLS94] have successfully removed the severe stability constraint (stiffness) by designing an efficient semi-implicit scheme based on a new reformulation of the problem. This reformulation employs a dynamic change of variables from the Cartesian coordinates (x, y) to the interface tangent angle and arclength metric. Using a *small scale decomposition* technique, one can separate the leading order operators that contribute to the stiffness. Moreover, the leading order singular terms are shown to be linear and have constant coefficients (in space). Thus, a Crank-Nicholson type discretization can be used to eliminate the stiffness of the time discretization. This reformulation greatly relaxes the stability constraint. Many interfacial problems that were previously unobtainable are now solvable using this method and new phenomena have been discovered.

In this paper, we apply this highly accurate and stable method to investigate the effect of small surface tension for several important interfacial flows. The first example is about the surface tension regularization effect for unstably stratified two-fluid interfaces. Without any physical regularization, the interface is subject

to the Rayleigh-Taylor instability and a curvature singularity may develop in finite time (see, e.g. [DR81, BMO80]). Our numerical results indicate that surface tension indeed regularizes the curvature singularity induced by the Rayleigh-Taylor instability and the interface rolls up into a spiral. However, the roll-up is terminated by the collision of the interface with itself, forming trapped bubbles of fluid at the core of the spiral. This process of bubble formation through self-intersection of a fluid interface has been observed by Hou, Lowengrub, and Shelley [HLS97] for a vortex sheet. Such pinching singularity is commonly observed in 3-D liquid jets where the azimuthal component of surface tension is believed to play an essential role in the collapsing process. However, this component is completely absent in a 2-D interface, making the appearance of such pinching singularities very surprising.

Our second example deals with the effect of small surface tension on the generation and structure of capillary waves on the surface of overturning water waves. The understanding of these short waves is important in the remote sensing of sea surface because the fine structure associated with short wavelengths scatters electromagnetic radiation. The phenomenon of capillary waves has been studied extensively in the literature (see, e.g. [LH95, LH96, Cra70, Tul96]). By using the stable spectrally accurate method discussed here, we are able to capture with high accuracy not only up to the appearance of the capillary jump [LH96], but also to follow the subsequent development of the small scale structure produced by the capillaries. Our numerical study also reveals certain scaling behavior of the capillary wavelength which agrees well with experimental observation [DQPW99]. The small-surface-tension solution is found to converge strongly to the zero-surface-tension solution.

Our third example is about the small surface tension limit of Hele-Shaw flows with suction. It is well known from laboratory experiments [Pat81] that Hele-Shaw flows with suction can develop long ‘fingers’ that encroach upon the viscous fluid being sucked. In the absence of surface tension, such fingering is not observed. Instead, solutions of the Hele-Shaw equations with suction are known to form finite-time cusp singularities before the fluid interface reaches the sink [HLO88, Ric72].

Here, we would like to investigate the limiting behavior of the small surface tension solution past the cusp singularity time t_c of the zero-surface-tension solution. Our computations show two surprising results. First, we find that an asymptotic corner angle is selected at the finger tip as it reaches the sink in the limit as surface tension tends to zero. This seems to be counter intuitive at first glance since one may think the tip angle would decrease with decreasing surface tension. Secondly, we find that the finger bulges and develops a neck singularity before it forms a wedge at the sink. This neck appears at a height close to that of the zero-surface-tension cusp. It is possible that the formation of this neck singularity is due to the influence of the zero-surface-tension singularity, and this pair of neck singularities may be responsible for the selection of the limiting wedge angle at the sink.

Our last example is on the singular perturbation of surface tension for Hele-Shaw problems. A natural conjecture is that the small-surface-tension solution would converge to the zero-surface-tension solution as surface tension tends to zero, provided that the zero-surface-tension solution is smooth (see e.g. [HLO88]). However, the asymptotic theory of Tanveer [Tan93] and Siegel, Tanveer, and Dai [STD96] suggests that the small surface tension limit could be singular for certain initial data even if the limiting zero-surface-tension solution is perfectly smooth. This possibility is quite surprising.

The numerical investigation of this question is very challenging. Since the zero-surface-tension problem is ill-posed, the numerical solution is extremely sensitive to noise for small surface tension [DS93, STD96]. We overcome this difficulty by using (i) a compact parametrization of the interface, (ii) a scaled equation for the perturbed quantity to factor out the small surface tension coefficient, and (iii) very high precision arithmetic. Using these techniques, we are able to compute accurately for extremely small values of surface tension. Our computations show convincingly that the small surface tension limit is indeed singular for certain initial data. The reason is that surface tension can introduce a new complex singularity at $t = 0^+$ which could subsequently impinge the physical domain at a time when the zero-surface-tension solution is still analytic. The impact of this so-called daughter singularity is to cause an indentation in the interface which subsequently evolves into a bulged finger. We also find that surface tension defines a length scale of the finger width.

All these calculations demand stable and highly accurate numerical methods. We also need to be extremely careful in controlling the noise effect to compute accurately the small surface tension limit and to capture the singular behavior of the solution. Although boundary integral methods are not general-purpose methods, they are especially suited for these types of challenging problems where extremely high resolution is needed. Grid-based methods, on the other hand, could have a lot of difficulties in achieving the same resolution. In addition, the inherent numerical diffusion or other artificial numerical regularizations could overshadow the small surface tension effect. In this sense, boundary integral methods provide an edge over other methods for accurate solution of this type of problems.

The rest of this paper is divided as follows. In Section 2, we describe the evolution equations of a fluid interface corresponding to two-fluid flows, water waves, and Hele-Shaw flows. The equations are presented in a boundary integral representation. Then, in Section 3, we discuss the stability of boundary integral methods for spatial discretizations. The technique to remove the surface tension induced stiffness is reviewed in Section 4. The four examples of numerical computations of interfacial flows with small surface tension are presented in Section 5.

2. General two-fluid interfaces

In this section, we provide the evolution equations in a boundary integral representation of three important examples of interfacial flows: water waves, stratified two-fluid interfacial flows, and Hele-Shaw flows. In the presence of small surface tension, intriguing and fascinating phenomena develop dynamically in this type of flows. The understanding of these phenomena has a fundamental impact in many physical and engineering applications. For example, capillary waves produced by surface tension are considered one of the key mechanisms for wave breaking and for the onset of turbulence. Moreover, the understanding of the fine scale structure generated by capillary waves is important in the remote sensing of the sea surface. On the other hand, stratified interfacial flows have been used as models to understand mixing of fluids, separation of boundary layers, generation of sounds (in bubbly flows), and coherent structures in turbulence models. Finally, theoretical and numerical studies of Hele-Shaw flows have received renewed interests and increasing attention in recent years because of the rich phenomena in the physical solutions and the potential applications in pattern formation and materials science.

2.1. Stratified two-fluid interfaces. We first consider the motion of general two-fluid interfacial flows in two space dimensions. The fluid on each side of the interface is assumed to be inviscid, incompressible, and irrotational. We denote the fluid quantities above the interface with the subscript 2 and those below the interface with subscript 1. In each fluid, the flow satisfies the Euler equations

$$\rho_i[\partial_t \mathbf{u}_i + (\mathbf{u}_i \cdot \nabla) \mathbf{u}_i] = -\nabla p_i - \rho_i g \hat{\mathbf{j}}, \quad i = 1, 2,$$

where ρ_i , \mathbf{u}_i , and p are the density, velocity, and pressure respectively. The constant g is the gravity acceleration. The incompressibility and irrotationality constraints imply that $\nabla \cdot \mathbf{u}_i = 0$ and $\nabla \times \mathbf{u}_i = 0$. At the interface, which we denote by Γ , we impose the Laplace-Young boundary condition which relates a pressure jump to the curvature of the interface κ by

$$[p]|_{\Gamma} = \tau \kappa,$$

where $[p]|_{\Gamma}$ denotes the jump of pressure across the interface Γ and τ is the surface tension coefficient. The normal velocity is assumed to be continuous across the interface. The tangential velocity at the interface in general is not uniquely defined since it may have a jump discontinuity across the interface. At any time t , we represent the interface parametrically by $(x(\alpha, t), y(\alpha, t))$, where α is a Lagrangian variable. The interface governing equation can be put in a convenient form by introducing the complex position variable $z(\alpha, t) = x(\alpha, t) + iy(\alpha, t)$. Of special interest is the case when the interface is a periodic perturbation of the flat interface, i.e. $z(\alpha, t) = \alpha + s(\alpha, t)$, where $s(\alpha, t)$ is a 2π -periodic function of α . Then, taking the tangential velocity to be the average of the limiting velocities above and below the interface, the interface evolves according to the so-called Birkhoff-Rott equation

$$(2.1) \quad \frac{d\bar{z}}{dt} = \frac{1}{2\pi i} \int_{-\pi}^{\pi} \gamma(\alpha') \cot \frac{1}{2}(z(\alpha) - z(\alpha')) d\alpha',$$

where we have used the periodic structure in s . Here, \bar{z} denotes the complex conjugate of z . The above integral should be understood as the Cauchy principal-value integral. The variable γ is the unnormalized vortex sheet strength, whose the evolution equation can be obtained from the Euler equations in both sides of the interface [BMO82]:

$$(2.2) \quad \frac{d\gamma}{dt} = -2A \left(\operatorname{Re} \left\{ \frac{d^2 \bar{z}}{dt^2} z_{\alpha} \right\} + \frac{1}{8} \partial_{\alpha} \left(\frac{\gamma^2}{|z_{\alpha}|^2} \right) + g y_{\alpha} \right) + S \kappa_{\alpha},$$

where $A = (\rho_1 - \rho_2)/(\rho_1 + \rho_2)$ is the Atwood number and $S = \tau/(\rho_1 + \rho_2)$ is a scaled surface tension parameter. The curvature κ is given by

$$\kappa = \frac{x_{\alpha} y_{\alpha\alpha} - x_{\alpha\alpha} y_{\alpha}}{(x_{\alpha}^2 + y_{\alpha}^2)^{3/2}}.$$

Equation (2.2) is a Fredholm integral equation of the second kind for $d\gamma/dt$. An important feature of this formulation is that it has a globally convergent Neumann series [BMO82]. As a result, the integral equation for $d\gamma/dt$ can be solved effectively by iteration. Equations (2.1) and (2.2) completely determine the motion of the interface.

2.2. Water wave equations. In the special case of water waves, we have $\rho_1 = 0$. The above derivation needs to be modified. Only the Bernoulli equation in the fluid region is needed to obtain an evolution equation for the potential. The first boundary integral method for water waves was proposed by Longuet-Higgins and Cokelet [LHC76] who used a single layer representation. This gives rise to a Fredholm integral equation of the first kind for $\frac{\partial \phi}{\partial n}$, which determines the normal velocity of the interface. The disadvantage of this approach is that the matrix associated with a Fredholm integral of the first kind is usually not well-conditioned and the number of iterations required increases rapidly with the number of the mesh points. The double layer representation introduced by Baker, Meiron, and Orszag [BMO82], on the other hand, does not have this disadvantage. Following [BMO82], we obtain a system of evolution equations given by:

$$(2.3) \quad \bar{z}_t = \frac{1}{4\pi i} \int_{-\pi}^{\pi} \gamma(\alpha') \cot \frac{1}{2}(z(\alpha) - z(\alpha')) d\alpha' + \frac{\gamma(\alpha)}{2z_\alpha(\alpha)} \equiv u - iv,$$

$$(2.4) \quad \phi_t = \frac{1}{2}(u^2 + v^2) - gy,$$

$$(2.5) \quad \phi_\alpha = \frac{\gamma}{2} + \operatorname{Re} \left(\frac{z_\alpha}{4\pi i} \int_{-\pi}^{\pi} \gamma(\alpha') \cot \frac{1}{2}(z(\alpha) - z(\alpha')) d\alpha' \right).$$

Here ϕ is the velocity potential and again γ denotes the vortex sheet strength. Equations (2.3)-(2.5) completely determine the motion of the system. Like the two-fluid interface problem, the integral equation for γ is a Fredholm integral equation of second kind which has a globally convergent Neumann series. Thus, γ can be solved efficiently by fixed point iteration.

2.3. Hele-Shaw flows. A closely related problem is the Hele-Shaw flow which describes a viscosity dominant creeping flow confined between two closely-spaced plates. The theoretical study in the West begins with Saffman and Taylor [ST58]. They found a family of exact self-similar finger-like solutions for the interface in a channel geometry without surface tension. Subsequent works have mostly focused on the role of surface tension in the selection of the finger width. Significant progress has been achieved in understanding steady states and their linear stability (see [Pel88] for a review). The dynamical behavior of Hele-Shaw flows has received a lot of interests inspired by the complex patterns formed by an expanding bubble. However, there are still many mysteries regarding the selection mechanism of finger widths for small surface tension.

Consider an interface Γ which separates two Hele-Shaw fluids of different viscosities and densities in a radial geometry. The velocity in each fluid is given by Darcy's law, together with the incompressibility constraint:

$$\mathbf{u}_j = -\frac{b^2}{12\mu_j} \nabla p_j, \quad \nabla \cdot \mathbf{u}_j = 0, \quad \text{for } j = 1, 2$$

Here b is the gap of the Hele-Shaw cell, μ_j , p_j , and ρ_j are the viscosity, pressure, and density on each side of the fluid interface. Nonlinearity comes through the boundary conditions. We impose again the Laplace-Young boundary condition which states that surface tension causes a jump in the pressure across the interface proportional to the local mean curvature. In addition, the normal velocity should be continuous at the interface.

We assume that there is a point sink (or a source) at the origin, inside a fluid blob. For large distances away from the sink, the velocity field tends to the simple radial flow:

$$(2.6) \quad \mathbf{u}(\mathbf{x}) \rightarrow Q \frac{\mathbf{x}}{|\mathbf{x}|^2}, \quad \text{as } |\mathbf{x}| \rightarrow \infty.$$

Here, Q is the suction rate (or pumping rate respectively) which is assumed constant and negative (positive).

Again, we represent the interface by the complex position variable $z(\alpha, t) = x(\alpha, t) + iy(\alpha, t)$. Unlike the fluid interface case, here we assume $z(\alpha, t)$ to be 2π -periodic in α . This implies that the interface Γ is a close curve. Denote the complex conjugate velocity by $W(\alpha, t) = u(\alpha, t) - iv(\alpha, t)$. This interface velocity can be represented by a boundary integral plus the sink contribution. Following [TA83, DS93], we can derive a boundary integral formulation given by:

$$(2.7) \quad \bar{z}_t = -\frac{1}{z(\alpha, t)} + \frac{1}{2\pi i} \int_0^{2\pi} \frac{\gamma(\alpha', t)}{z(\alpha, t) - z(\alpha', t)} d\alpha',$$

$$(2.8) \quad \gamma = 2A_\mu \operatorname{Re} \left(-\frac{z_\alpha(\alpha, t)}{z(\alpha, t)} + \frac{z_\alpha(\alpha, t)}{2\pi i} \int_0^{2\pi} \frac{\gamma(\alpha', t)}{z(\alpha, t) - z(\alpha', t)} d\alpha' \right) + S\kappa_\alpha,$$

where $A_\mu = (\mu_1 - \mu_2)/(\mu_1 + \mu_2)$ is the viscosity Atwood ratio and $S = \frac{b^2}{12\bar{\mu}}\tau$ is a scaled surface tension parameter. We nondimensionalize the equations of motion by taking the initial blob radius to be 1 and by setting $Q = -1$.

3. Stability of boundary integral methods

In this section, we review some stability issues of boundary integral methods for interfacial flows. We use the water wave problem as an example to illustrate the main ideas. The complete stability analysis of the boundary integral method for water waves was performed by Beale, Hou, and Lowengrub [BHL96]. Cenicerros and Hou analyzed the more general two-fluid interfacial flow with surface tension [CH98].

Numerical methods can be readily derived from the boundary integral formulation of water waves by choosing a discretization for the principal-value integral and for the spatial derivative. A classical discretization for the integral is the point vortex method introduced by Rosenhead [Ros32], while a popular choice for the derivative is the cubic spline approximation. However, numerical simulations using boundary integral methods are known to be sensitive to numerical instabilities [LHC76, Rob83, Dol92]. This includes some of the existing boundary integral methods. In order to avoid numerical instability, a certain compatibility between the choice of quadrature rule for the singular integral *and* the discrete derivatives must be satisfied. This compatibility ensures that a delicate balance of terms that holds on the continuous level is preserved on the discrete level. This point will be further illustrated below.

Let $z_j(t)$ be the numerical approximation of $z(\alpha_j, t)$, where $\alpha_j = jh$, $h = 2\pi/N$ and N is the number of discrete points on the interface. $\phi_j(t)$ and $\gamma_j(t)$ are defined similarly. To approximate the velocity integral, we use the alternating

point trapezoidal rule:

$$\int_{-\pi}^{\pi} \gamma(\alpha') \cot \frac{1}{2}(z(\alpha_j) - z(\alpha')) d\alpha' \simeq \sum_{\substack{k=-N/2+1 \\ (j-k) \text{ odd}}}^{N/2} \gamma_k \cot \frac{1}{2}(z_j - z_k) 2h .$$

The advantage of using this quadrature is that the approximation is spectrally accurate(see, e.g. [She92]). Let us denote by D_h the discrete derivative operator. It is convenient for the analysis to define D_h through its spectrum property: $\widehat{(D_h)_k} = ik\rho(kh)$ where the over-caret stands for the Fourier transform and ρ is some nonnegative even function. The specific form of $\rho(kh)$ depends on the approximation. For example, we have $\rho(kh) = 3 \sin(kh)/(kh(2 + \cos(kh)))$ for the cubic spline approximation and $\rho(kh) = 1$ for the pseudo-spectral derivative.

Now we can present our numerical algorithm [BHL96] for the water wave equations (2.3)-(2.5) as follows:

$$(3.1) \quad \frac{d\bar{z}_j}{dt} = \frac{1}{4\pi i} \sum_{\substack{k=-N/2+1 \\ (j-k) \text{ odd}}}^{N/2} \gamma_k \cot \frac{1}{2}(z_j^{(\rho)} - z_k^{(\rho)}) 2h + \frac{\gamma_j}{2D_h z_j} \equiv u_j - iv_j,$$

$$(3.2) \quad \frac{d\phi_j}{dt} = \frac{1}{2}(u_j^2 + v_j^2) - gy_j ,$$

$$(3.3) \quad D_h \phi_j = \frac{\gamma_j}{2} + \text{Re} \left(\frac{D_h z_j}{4\pi i} \sum_{\substack{k=-N/2+1 \\ (j-k) \text{ odd}}}^{N/2} \gamma_k \cot \frac{1}{2}(z_j^{(\rho)} - z_k^{(\rho)}) 2h \right) ,$$

where $z^{(\rho)}$ denotes a Fourier filtering applied on z and defined as $z^{(\rho)} = \alpha + s^{(\rho)}$ with $\widehat{(s^{(\rho)})_k} = \hat{s}_k \rho(kh)$. The filtered quantity $z^{(\rho)}$ in (3.1) and (3.3) is to balance the high frequency errors introduced by D_h . This will become apparent in the discussion of stability below.

Theorem 1[BHL96]. *Assume that the water wave problem is well-posed and has a smooth solution in C^{m+2} ($m \geq 3$) up to time T . Then if D_h corresponds to a r -th order derivative approximation, we have for $0 < h \leq h_0(T)$*

$$(3.4) \quad \|z(t) - z(\cdot, t)\|_{l^2} \leq C(T)h^r .$$

Similar convergent results hold for ϕ_j and γ_j . Here $\|z\|_{l^2}^2 = \sum_{j=1}^N |z_j|^2 h$.

3.1. Discussion of stability analysis. Here, we discuss some of the main ingredients in the stability analysis of the scheme given by (3.1)-(3.3). We will mainly focus on linear stability. Once linear stability is established, nonlinear stability can be obtained relatively easily by using the smallness of the error and an induction argument. The reader is referred to [BHL96] for details.

The goal is to derive evolution equations for the errors $\dot{z}_j(t) \equiv z_j(t) - z(\alpha_j, t)$, etc., and to estimate their growth in time. To simplify the stability analysis, we expand the periodic sum into an infinite sum over the whole line, i.e.

$$\frac{1}{2} \sum_{\substack{k=-N/2+1 \\ (j-k) \text{ odd}}}^{N/2} \gamma_k \cot \frac{1}{2}(z_j^{(\rho)} - z_k^{(\rho)}) 2h = \sum_{(j-k) \text{ odd}} \frac{\gamma_k}{z_j^{(\rho)} - z_k^{(\rho)}} 2h \equiv W_j .$$

Let us now define

$$(3.5) \quad \dot{W}_j = W_j - \sum_{(j-k) \text{ odd}} \frac{\gamma(\alpha_k)}{z(\alpha_j)^{(\rho)} - z(\alpha_k)^{(\rho)}} 2h.$$

\dot{W}_j can be written as the sum of linear terms in \dot{z}_j and $\dot{\gamma}_j$ plus nonlinear terms. We find that

$$(3.6) \quad \begin{aligned} \dot{W}_j &= \frac{h}{\pi i} \sum_{(j-k) \text{ odd}} \frac{\dot{\gamma}_k}{z(\alpha_j)^{(\rho)} - z(\alpha_k)^{(\rho)}} \\ &- \frac{h}{\pi i} \sum_{(j-k) \text{ odd}} \frac{\gamma(\alpha_k)(\dot{z}_j^{(\rho)} - \dot{z}_k^{(\rho)})}{(z(\alpha_j)^{(\rho)} - z(\alpha_k)^{(\rho)})^2} + \text{nonlinear terms.} \end{aligned}$$

Next, we use the Taylor expansion for the singular kernel to obtain the most singular contributions and write

$$(3.7) \quad \frac{1}{z(\alpha_j) - z(\alpha_k)} = \frac{1}{z_\alpha(\alpha_j)(\alpha_j - \alpha_k)} + f(\alpha_j, \alpha_k),$$

where f is a smooth function. Thus, the leading order contribution to the first term in (3.6) is $(2iz_\alpha)^{-1}H_h\dot{\gamma}_j$, where H_h is the discrete Hilbert transform defined as

$$(3.8) \quad H_h(\dot{\gamma}_j) \equiv \frac{1}{\pi} \sum_{(j-k) \text{ odd}} \frac{\dot{\gamma}_k}{\alpha_j - \alpha_k} 2h.$$

The remaining term involving the smooth kernel f becomes a smoothing operator A_{-1} of order one, i.e., $D_h A_{-1} = A_0$ and $A_{-1} D_h = A_0$, where A_0 denotes a bounded operator from l^p to l^p . Similarly, the most important contribution to the second term in (3.6) is $-\gamma(2iz_\alpha^2)^{-1}\Lambda_h(z_j^{(\rho)})$, where Λ_h is defined as follows:

$$(3.9) \quad \Lambda_h(\dot{f}_j) \equiv \frac{1}{\pi} \sum_{(j-k) \text{ odd}} \frac{\dot{f}_j - \dot{f}_k}{(\alpha_j - \alpha_k)^2} 2h.$$

Denote by H and Λ the corresponding continuous operators for H_h and Λ_h respectively, i.e.

$$H(f) = \frac{1}{\pi} \int \frac{f(\alpha')}{\alpha - \alpha'} d\alpha', \quad \Lambda(f) = \frac{1}{\pi} \int \frac{f(\alpha) - f(\alpha')}{(\alpha - \alpha')^2} d\alpha'.$$

It is easy to verify using integration by parts that

$$(3.10) \quad \Lambda(f) = H(D_\alpha f),$$

where D_α is the continuous derivative operator. Our analysis indicates that a similar compatibility condition must be satisfied among the discrete operators H_h , Λ_h , and D_h to maintain numerical stability, i.e.

$$(3.11) \quad \Lambda_h(\dot{z}_i) = H_h D_h(\dot{z}_i),$$

for \dot{z} satisfying $\widehat{\dot{z}}_0 = \widehat{\dot{z}}_{N/2} = 0$. Unfortunately, many existing boundary integral methods violate this compatibility condition, and consequently are subject to numerical instability.

An important question is how to modify our discretization to obtain a stable method. One way to do this is to introduce appropriate Fourier filtering in the approximations of the velocity integral as we have done in (3.1) and (3.3). By

doing this, we can ensure that a variant of the compatibility condition (3.11) is satisfied:

$$(3.12) \quad \Lambda_h(\dot{z}_j^{(\rho)}) = H_h D_h(\dot{z}_j).$$

We can verify this from the spectrum properties of H_h and Λ_h and the definitions of D_h and the ρ filtering. With this modified compatibility condition, we can obtain stability of our boundary integral method.

To complete our stability analysis, we need to make use of the following properties of the discrete Hilbert transform: (i) $H_h^2 = -I$, (ii) $\Lambda_h(z^{(\rho)}) = H_h D_h(z)$, (iii) the commutator, $[H_h, f] \equiv H_h f - f H_h$, is a smoothing operator, i.e. $[H_h, f](\dot{z}^{(\rho)}) = A_{-1}(\dot{z})$ for smooth f . Following the linear well-posedness analysis, we can derive an error equation for \dot{z}_j as follows (see [BHL96])

$$\frac{d\dot{z}_j}{dt} = \frac{1}{z_\alpha(\alpha_j)} (I - iH_h) D_h \dot{F}_j + A_0(\dot{z}_j) + A_{-1}(\dot{\phi}_j) + O(h^r),$$

where $\dot{F}_j = \dot{\phi}_j - u(\alpha_j)\dot{x}_j - v(\alpha_j)\dot{y}_j$. At this point, it is essential to project the error equation into the local tangent and normal vectors of the underlying interface, $z(\alpha, t)$. In this local coordinate, the error equations are greatly simplified and the stability analysis becomes apparent. Alternatively, the local tangent angle to the interface has also been shown [CH98] to be a natural variable for the stability analysis, specially in the presence of surface tension.

Denote by \dot{z}_j^N and \dot{z}_j^T the normal and tangential components of \dot{z}_j , with respect to the underlying interface $z(\alpha_j, t)$ and let $\hat{\mathbf{n}}$ be the outward unit normal. We further make the following change of variables $\dot{\delta}_j = \dot{z}_j^T + H_h \dot{z}_j^N$. We obtain after some simplification that

$$(3.13) \quad \frac{d\dot{\delta}_j}{dt} = A_{-1}(\dot{F}_j) + A_0(\dot{z}_j),$$

$$(3.14) \quad \frac{d\dot{z}_j^N}{dt} = \frac{1}{|z_\alpha(\alpha_j)|} H_h D_h \dot{F}_j + A_{-1}(\dot{F}_j) + A_0(\dot{z}_j),$$

$$(3.15) \quad \frac{d\dot{F}_j}{dt} = -c(\alpha_j, t)\dot{z}_j^N + A_{-1}(\dot{z}_j), \quad c(\alpha, t) = (u_t, v_t + g) \cdot \hat{\mathbf{n}},$$

where equation (3.15) is obtained by performing error analysis on Bernoulli equation and by using the Euler equations. In this form it is clear that only the normal component of \dot{z}_j is important. This is consistent with the physical property of interfacial dynamics. The leading error equations now become so simple that an energy estimate can be easily carried out. Note that $H_h D_h$ is a positive operator with a Fourier symbol $\rho(kh)|k|$. The discretization is stable if the water wave problem is well-posed, i.e., the sign condition $c(\alpha, t) > 0$ is satisfied. We refer to [BHL96] for details.

Generalization of the above stability analysis to 3-D interfacial flows proves to be quite challenging due to the non-removable branch point singularity in the 3-D boundary integral kernel. Nevertheless, substantial progress has been made recently by Beale [Bea98] and by Hou and Zhang [HZa, HZb] in designing stable 3-D boundary integral methods for water waves. These analyses also shed new light into the 2-D interface problems. Since these stabilized methods are quite sophisticated, we will omit their discussion here.

4. Removing the stiffness of surface tension for interfacial flows

Surface tension at an interface between two immiscible fluids arises from the imbalance of their intermolecular cohesive forces. It is one of the most commonly used physical regularizations in the study of interfacial flows. Surface tension plays an important role in understanding fluid phenomena such as pattern formation in Hele-Shaw cells, the motion of capillary waves on free surfaces, and the formation of fluid droplets. Although surface tension provides a natural physical regularization for fluid interfaces, it also induces a severe time step stability constraint for explicit numerical methods. This severe stability constraint, which we refer to as stiffness, is introduced by surface tension through the high order spatial derivatives in the local curvature. These high order derivatives couple to the interface evolution equation in a nonlinear and nonlocal manner. If an explicit time integration method is used, these terms produce strong stability constraints on the time step (for the Hele-Shaw flows, the time stability constraint is $S\Delta t \leq \min_\alpha |z_\alpha| h^3$). Moreover, these constraints are generally time dependent, and become more severe by the differential clustering of points along the interface. This has been one of the major difficulties in simulating interfacial flows with surface tension.

Hou, Lowengrub, and Shelley (HLS) [HLS94] have developed an efficient method to remove the stiffness induced by surface tension for 2-D fluid interfaces. Their method is based on a *small scale decomposition* technique and on a reformulation of the problem in terms of the local tangent angle θ at the interface and arclength metric $s_\alpha = \sqrt{x_\alpha^2 + y_\alpha^2}$. The main motivation of using these new dependent variables is that curvature has a very simple expression in these variables: $\kappa = \theta_\alpha / s_\alpha$. Another important observation is that the stiffness only arises at small scales. Moreover, the leading order contribution of the singular integral operator at small scales can be expressed in terms of the Hilbert transform, which is diagonalizable in Fourier space. By treating only the leading order terms implicitly, but treating the lower order terms explicitly, an efficient semi-implicit discretization which effectively removes the stiffness of surface tension can be obtained.

We will now give a brief description of the method. Given an equation of motion of a free interface,

$$(x_t(\alpha, t), y_t(\alpha, t)) = U\hat{\mathbf{n}} + T\hat{\mathbf{s}},$$

it can be recast in terms of the variables θ and s_α , and the following evolution equations can be easily obtained:

$$(4.1) \quad (s_\alpha)_t = T_\alpha - \theta_\alpha U,$$

$$(4.2) \quad \theta_t = \left(\frac{1}{s_\alpha}\right) (U_\alpha + \theta_\alpha T),$$

where $\hat{\mathbf{n}}$ and $\hat{\mathbf{s}}$ are the unit local normal and tangential vectors respectively. U and T are the local normal and tangential components of the interface velocity. Note that only the normal velocity is physically prescribed. The tangential velocity would determine the parametrization of the interface, but it does not affect the shape of the interface. This degree of freedom in choosing T is exploited to derive a simpler evolution equation for s_α and θ . One possible choice of T is to enforce α to be an arclength variable, which implies that s_α is independent of α if it is so

initially. To achieve this, the tangential velocity T is selected as follows:

$$(4.3) \quad T(\alpha, t) = T(0, t) + \int_0^\alpha \theta_{\alpha'} U d\alpha' - \frac{\alpha}{2\pi} \int_0^{2\pi} \theta_{\alpha'} U d\alpha'.$$

This equation expresses T entirely in terms of θ and U . With this tangential velocity, the evolution equations for θ and s_α reduce to

$$(4.4) \quad (s_\alpha)_t = -\frac{1}{2\pi} \int_0^{2\pi} \theta_\alpha U d\alpha.$$

$$(4.5) \quad \theta_t = \left(\frac{1}{s_\alpha} \right) (U_\alpha + \theta_\alpha T) .$$

This system should be solved together with the evolution equations governing other dynamical variables, such as the vortex sheet strength or the velocity potential. This is a complete reformulation of the interface evolution problem.

The next step in the method of HLS is to extract the leading order singular operators that contribute to the numerical stiffness. Again, a Taylor expansion of the singular kernel is performed as in (3.7). For smooth interfaces, only the singular term on the right hand side of (3.7) contributes to the stiffness. The smooth kernel f gives rise to a smoothing operator which decays rapidly in high frequency, consequently it does not contribute to the stiffness. Thus, the leading order of the normal velocity U at small scales becomes

$$U \sim \frac{1}{2} \left(\frac{2\pi}{s_\alpha} \right) \mathcal{H}[\gamma] .$$

In the case of two-fluid interface motion, we need to get the leading order term for the vortex sheet strength γ . This term clearly comes from the curvature which introduces the highest order spatial derivatives. Therefore

$$\gamma_t \sim S \kappa_\alpha .$$

After singling out the leading order terms, the system for θ and γ is decomposed as follows:

$$(4.6) \quad \theta_t = \left(\frac{1}{2s_\alpha^2} \right) \mathcal{H}[\gamma_\alpha] + P ,$$

$$(4.7) \quad \gamma_t = \left(\frac{S}{2s_\alpha} \right) \theta_{\alpha\alpha} + Q ,$$

where P and Q represent the smoother and lower order terms. They are obtained by subtracting off the leading order terms from the right hand sides of the θ and γ equations respectively. We refer to this technique as the *Small Scale Decomposition* (SSD). A similar but simpler, SSD can be found for Hele-Shaw flows. Hou, Klapper, and Si [HKS98] have extended this technique to remove the stiffness of curvature in 3-D filaments.

It is important to note that the leading order linear operators can be diagonalized under Fourier transform. An efficient semi-implicit scheme can be easily designed by discretizing the leading order stiff terms implicitly using a Crank-Nicholson discretization, and leap-frogging on the lower order terms. Let $L(t) = 2\pi s_\alpha$ which represents the total arclength of the interface. In Fourier space, (4.6)

and (4.7) become

$$(4.8) \quad \frac{\hat{\theta}^{n+1} - \hat{\theta}^{n-1}}{2\Delta t} = \frac{|k|}{4} \left(\left(\frac{2\pi}{L^{n+1}}\right)^2 \hat{\gamma}^{n+1} + \left(\frac{2\pi}{L^{n-1}}\right)^2 \hat{\gamma}^{n-1} \right) + \hat{P}^n(k)$$

$$(4.9) \quad \frac{\hat{\gamma}^{n+1} - \hat{\gamma}^{n-1}}{2\Delta t} = -\frac{S}{2} k^2 \left(\frac{2\pi}{L^{n+1}} \hat{\theta}^{n+1} + \frac{2\pi}{L^{n-1}} \hat{\theta}^{n-1} \right) + \hat{Q}^n(k).$$

Note that there is no stiffness in the ODE for $L(t)$ so we can discretize L explicitly. Once L^{n+1} is updated, $\hat{\theta}^{n+1}(k)$ and $\hat{\gamma}^{n+1}(k)$ can be found by inverting a 2×2 matrix. This gives rise to a semi-implicit scheme which is at the same cost of an explicit scheme but with no high order stability constraint. It is also possible to design a fourth order semi-implicit discretization based on the same idea. This has been used effectively in many applications, including those to be described in the next section.

5. Numerical Study of Interfacial Flows

We now apply the methods reviewed in the previous sections to investigate numerically interfacial flows with small surface tension. We consider three examples. In the first one, we investigate the surface tension stabilizing effect for unstably stratified two-fluid interfaces. In the second example we study the dynamic generation of capillary waves in overturning water waves with small surface tension. The third example is devoted to the study of a Hele-Shaw flow with suction in the limit of small surface tension. In addition, we review an innovative method to study the singular perturbation of surface tension and the effect of noise in Hele-Shaw flows and present surprising numerical results. All these studies reveal some fascinating singular limiting behaviors of the interfacial flows as surface tension tends to zero.

5.1. Unstably stratified two-fluid interfacial flows. One of the classical examples of hydrodynamic instability occurs when a layer of heavy fluid sits on top of a lighter fluid, or equivalently when the interface is accelerated toward the heavy fluid. This is called Raleigh-Taylor Instability [DR81]. Rayleigh-Taylor instability is a fundamental instability of incompressible fluid flow at high Reynolds number. The idealization of an unstably stratified shear layer as a two-fluid interface separating two regions of potential flow has often been used as a model to study mixing properties, boundary layers and coherent structures of fluids.

Pullin [Pu182] was one of the first to study numerically the stabilizing effect of surface tension for unstably stratified two-fluid interfaces. But due to the inherent numerical instability, Pullin's computations were not conclusive. Rangel & Sirignano [RS88] also studied the effect of surface tension and density ratio on the nonlinear growth of the Kelvin-Helmholtz instability. To overcome the time-step stiffness constraint, they redistributed their grid points every time step. While this technique can effectively relax the time step stability constraint, it also introduces excessive numerical diffusion which could overshadow the effect of surface tension.

In [CH98], we computed several examples of two-fluid interfacial flows in the presence of surface, including the particular case we present now. We consider here an unstably stratified two-fluid interfacial flow (corresponding to $Ag < 0$) with the following initial data

$$\begin{aligned} z(\alpha, 0) &= \alpha + 0.1i \cos(2\pi\alpha), \\ \gamma(\alpha, 0) &= 0. \end{aligned}$$

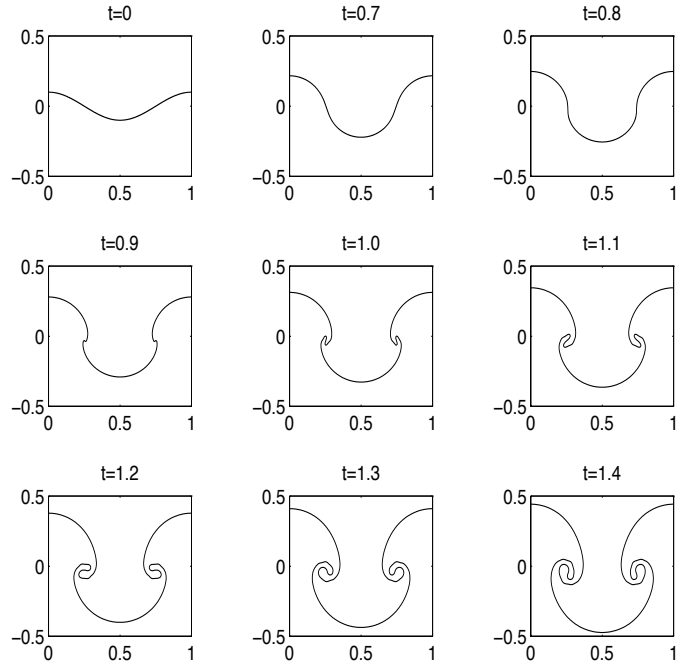


FIGURE 1. Unstably stratified flow: Time evolution of the interface with $A = -0.1$ and $S = 0.005$. $N = 1024$ and $\Delta t = 2.5 \times 10^{-4}$.

In Figure 1 we plot the time evolution of an interface with $A = -0.1$, $g = 10$, and $S = 0.005$. For this calculation we use $N = 1024$ and $\Delta t = 2.5 \times 10^{-4}$. We observe two small fingers that appear around $t = 0.9$, and the interface begins to roll up. One can also see some capillary waves that are generated around $t = 1.2$ and move outwards from the centers of roll-up. To ensure that our calculations are accurate, we perform a careful resolution study. We find that up to $t = 1.4$, the accuracy stays at about 4.66 digits for $N = 1024$ and about 7.2 digits for $N = 2048$. With $N = 2048$, we can continue our computations with reasonably good accuracy. In Figure 2, we plot a sequence of the interface position in time from $t = 1.5$ to $t = 1.75$. Note that the finger tips broaden as they continue to roll, and that the interface bends towards the finger tips. At $t = 1.75$, the minimum distance between the finger tip and the opposite side of the interface is about 0.016. The minimum distance continues to approach zero and by $t = 1.785$ (Figure 3(a)), is approximately 5×10^{-4} .

This process of bubble formation through self-intersection of a fluid interface has been observed by HLS [HLS97] for a vortex sheet. The vortex sheet problem is relatively easier to compute than the two-fluid interface here because the vortex sheet strength, γ , can be determined dynamically without having to invert an integral equation iteratively. HLS also used adaptive mesh refinement which improved the local resolution near the singularity. Based on their numerical results and a local model, HLS have suggested that the interface minimum separation decreases to zero according to $(t_c - t)^{2/3}$. In Figure 3(b), we compare the computed minimum distance d_i , represented as circles in the plot, and a fitted curve of the form $d(t) = C(t_c - t)^{2/3}$ as a solid line. We can clearly see a good agreement between

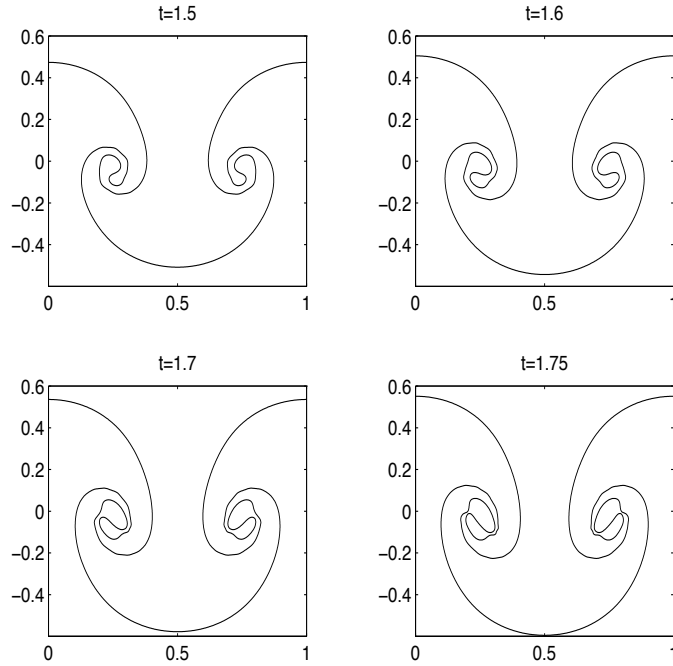


FIGURE 2. Unstably stratified flow: $A = -0.1$ and $S = 0.005$. Sequence of interface positions. $N = 2048$ and $\Delta t = 1.25 \times 10^{-4}$.

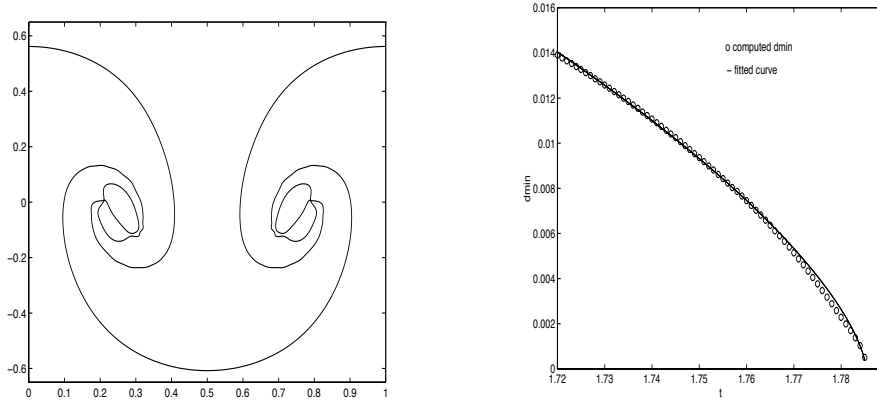


FIGURE 3. Unstably stratified flow: $A = -0.1$ and $S = 0.005$. (a) Interface position at $t = 1.785$ and (b) minimum separation against time. The circles represent the computed values and the solid line a fitted curve of the form $d(t) = C(t_c - t)^{2/3}$.

the values d_i and $d(t_i)$ up to $t = 1.76$. Beyond which, our calculations are not well resolved.

If the interface indeed goes through a self-intersection, this constitutes a singularity in the evolution. We believe that the collision of the interface is caused by the creation of intense localized jets produced by surface tension. Our numerical results

indicate that the curvature blows up at the time of the collision and the interface forms corners. This collision may signal an imminent change in the topology of the flow. Such topological singularity is commonly observed in interfacial flows, e.g. in three-dimensional liquid jets. For three-dimensional liquid jets, the azimuthal component of surface tension is believed to play an essential role in driving the jet to form a pinching singularity. However, this component is completely absent in the two-dimensional unstably stratified interfacial flow we study here, making the appearance of such pinching singularities very surprising.

5.2. Dynamic generation of capillary waves. Unsteady motion of water waves is one of the most familiar examples of free surfaces in our everyday experience. It is also the source of many interesting nonlinear phenomena. An important event is the generation of capillary waves on the forward wave front [DQPW99, EKT87, PLT93]. Surface tension is believed to play a fundamental role in generating these capillary waves.

The phenomenon of capillary waves generated by steady steep gravity waves has been studied systematically by a number of researchers (see e.g. [LH95, LH96, Cra70]). The effects of surface tension on breaking waves have recently been addressed by Tulin [Tul96]. The careful simulations by Tulin show the appearance of a capillary jump, as defined by Longuet-Higgins [LH96], near the wave crest. Recent computations by the authors [CH99] using the stable spectrally accurate method discussed here, reveal a more detailed structure of the capillaries. As we show next, we are able to compute with high accuracy not only up to the appearance of the capillary jump as observed by Tulin, but also to follow the subsequent development of the small scale structure produced by the capillaries. We also examine the limiting behavior of the capillary waves as surface tension decreases to zero.

Our initial data is the following:

$$(5.1) \quad z(\alpha, 0) = \alpha + 0.1i \cos(2\pi\alpha) ,$$

$$(5.2) \quad \gamma(\alpha, 0) = -1 + 0.1 \sin(2\pi\alpha) .$$

The nonzero mean in γ corresponds to a nonzero velocity (equal to $-1/2$) at $y = -\infty$. This gives the wave an impulse to cause it to overturn. We take $g = 10$ and vary the surface tension coefficient S throughout the simulations. Our first simulation is for $S = 0.001$. In Figure 4, we present the interface profile at times $t = 0, 0.30$, and 0.45 , computed using $N = 2048$ and $\Delta t = 5 \times 10^{-5}$. We can see that the interface becomes vertical at $t = 0.30$ and a capillary wave appears soon after the wave begins to overturn. Figure 5(a) gives a close-up of a neighborhood of the crest at time $t = 0.45$. The curvature in this region is plotted in Figure 5(b). We can clearly see a capillary wave train. We also examine closely the onset of this capillary wave and find that at $t = 0.26$, the curvature develops a spike right after the wave tip. Such spike is not present in the case $S = 0$ for which the curvature varies smoothly in the entire region. This spike subsequently develops into the capillary wave train.

A closer look at the interface profiles near $t = 0.45$ (Figure 5(a)) shows that the capillary trough gets narrower in time, suggesting a possible formation of a trapped bubble through self-intersection of the interface. We also find that both the curvature and its derivative have maxima (in absolute value) in a small neighborhood about the edge.

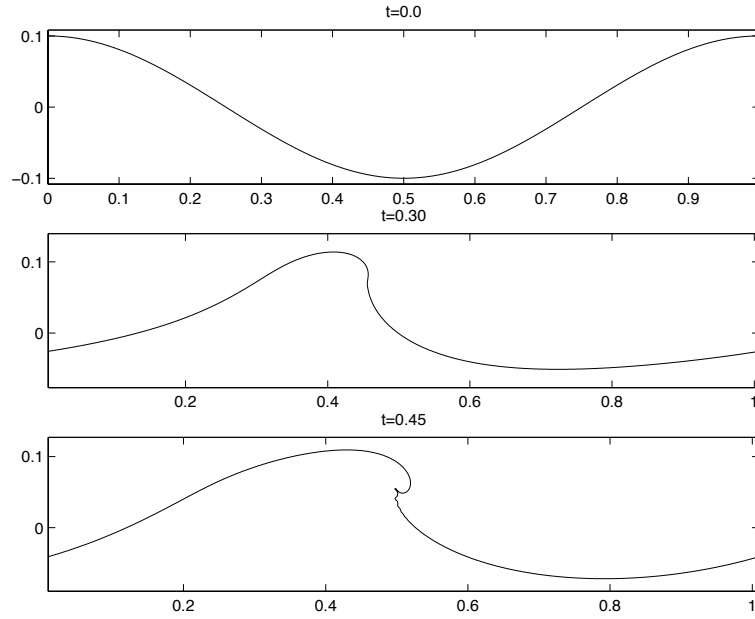


FIGURE 4. Breaking wave profiles for $S = 0.001$ at times $t = 0$, 0.30 , and 0.45 . $N = 2048$ and $\Delta t = 5 \times 10^{-5}$.

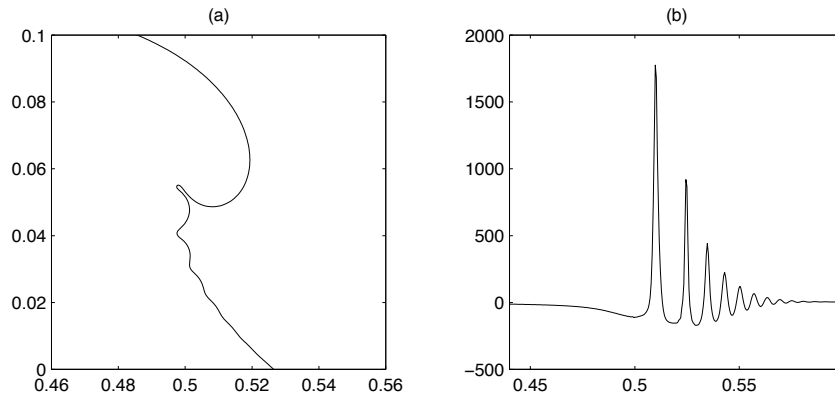


FIGURE 5. (a) Close-up of the interface at $t = 0.45$ and (b) the curvature plotted against the Lagrangian parameter α for $S = 0.001$, $N = 2048$, and $\Delta t = 5 \times 10^{-5}$.

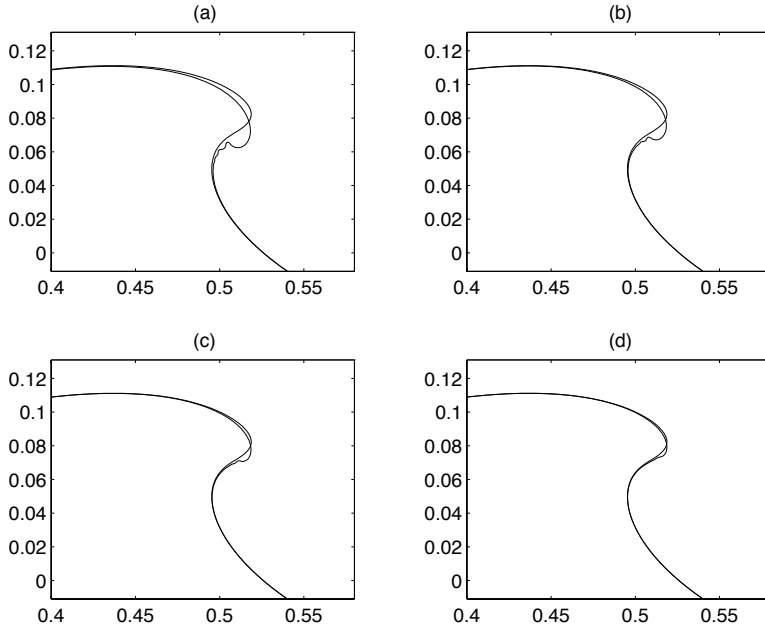


FIGURE 6. Comparison of the zero surface tension interface profile with the $S > 0$ profiles as S is decreased at $t = 0.45$. (a) $S = 2.5 \times 10^{-4}$. (b) $S = 1.25 \times 10^{-4}$. (c) $S = 6.25 \times 10^{-5}$. (d) $S = 3.125 \times 10^{-5}$.

We investigate how the capillary wavelength, denoted as λ_S , and its amplitude, denoted as a_S , scale with S as S is decreased. The capillary wavelength is defined as the distance between the two largest values of $|\kappa|$. Although it is difficult to obtain an accurate scaling for λ_S and a_S , we find that for a fixed time, both quantities decrease nonlinearly as S decreases to zero. The scaling for λ_S is roughly $O(\sqrt{S})$. This seems to be in agreement with the experimental results of Duncan *et al.* [DQPW99]. The monotonely decreasing behavior of λ_S and a_S suggests that the limiting solutions converge strongly to the $S = 0$ profile for a fixed time. This is indeed the case. We see from Figure 6 that the interface profiles with decreasing surface tensions converge to the zero-surface-tension profile at the fixed time $t = 0.45$. This should be expected since the limiting zero-surface-tension water wave problem is well-posed, even after the wave overturns [Wu97]. Surface tension acts as a regular perturbation in this case. As we will see in the last subsection, this conclusion does not apply to the ill-posed Hele-Shaw problem.

5.3. Hele-Shaw flow with suction. Here, we would like to investigate the small surface tension limit of the Hele-Shaw flow with suction. This is a challenging problem because the zero-surface-tension problem is ill-posed. There are limited existence results of Hele-Shaw solutions in the presence of surface tension. Short-time existence has been obtained by Duchon-Robert [DR84]. There is also a long-time existence result but near equilibrium and without suction by Constantin and Pugh [CP93]. Tian [Tia95] shows that singularity formation is inevitable if the center of the viscous blob is not at the sink. However, the type of singularity is

still unknown. On the other hand, there has been some attempt to perform a perturbation analysis of the small surface tension solution using the knowledge of the zero-surface-tension solutions. In [HLO88], Howison, Lacey, and Ockendon propose an asymptotic model by assuming the existence of a self-similar steady-state solution. Their analysis predicts that small surface tension could cause the interface in the neighborhood of the cusp to propagate rapidly as a narrow jet, analogous to a thin crack. They termed this the 'crack' model. However, since existence of this self-similar steady-state solution is unknown, the validity of this asymptotic result is still in doubt.

To investigate the asymptotic behavior as surface tension tends to zero, we consider an initially circular blob of viscous fluid surrounded by inviscid fluid, i.e., $A_\mu = 1$. The center of the initial blob is located at $(0, -0.1)$ and the sink is placed at the origin. All the computations presented here are performed in double precision. Due to the ill-posedness of the zero-surface-tension Hele-Shaw problem, it is necessary to use Krasny filtering [Kra86] to suppress the spurious growth of the round-off error. Krasny filtering is a simple but effective numerical filter which sets to zero all the Fourier modes of the solution whose magnitude are below certain filter level. In our computations we set this filter level to be 10^{-12} .

Due to the singular nature of the small surface tension solution, extremely high space and time resolutions are required to obtain accurate numerical solutions. Initially, we use $N = 2048$ for most of the computations. We double N as soon as the magnitude of the highest frequency mode of the tangent angle $\theta(\alpha, t)$ is greater than the filter level. Since the interface propagates rapidly to the sink, very small values of time step Δt are required to compute accurately the interface motion as it approaches the sink. At the latest stage of the motion, the number of grid points typically increases to $N = 8192$ or $N = 16384$ and $\Delta t = 2 \times 10^{-7}$. We remark that Kelly and Hinch [KH97] have studied numerically the effects of surface tension on the Hele-Shaw flow with suction. By using a different boundary integral method with a maximum of 200 grid points which are redistributed dynamically, their computations lack the high accuracy necessary to capture the interface behavior for sufficiently small surface tension. Nie and Tian [NT98] have performed a careful numerical study of this problem and found that the flow develops a curvature singularity (in the form of a corner) when the interface reaches the sink. However, their study is restricted to large surface tension case, and does not address the limiting behavior of the small-surface-tension solution.

In the absence of surface tension, our computation shows that the interface develops a cusp singularity at $t_c = 0.2842$ and is located at $(0, 0.2305)$ for this particular initial data. With surface tension $S = 5 \times 10^{-5}$, we can compute beyond the cusp singularity of the zero-surface-tension solution. Figure 7 shows the interface shape for $S = 5 \times 10^{-5}$. We clearly see that the finger bulges and develops a well-defined neck before it forms a wedge. It is interesting to note that this neck appears at a height close to that of the zero-surface-tension cusp. It is reasonable to conjecture that the formation of the neck and the bulging of the finger are due to the influence of the zero-surface-tension singularity.

We consider now the limiting behavior of the interface past t_c as surface tension is decreased. We find with surprise that an asymptotic corner angle is selected in the limit as surface tension tends to zero when the finger tip is about to reach the sink. To validate this finding, we compare the interfaces for a set of decreasing values of surface tension. Since the velocity of the interface depends on surface tension, it

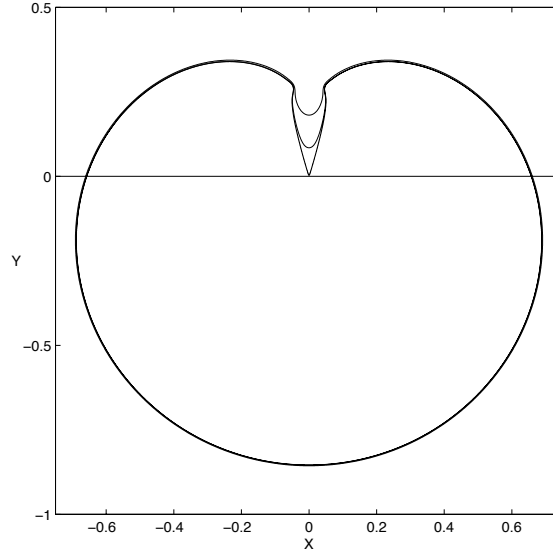


FIGURE 7. Evolution of the initially circular fluid blob past t_c , for $S = 5 \times 10^{-5}$. The interface is plotted at $t = 0.2880, 0.2900$, and 0.29181 . $N = 16384$ and $\Delta t = 2 \times 10^{-7}$ for the last stage of the motion

S	Wedge angle	Variation
8×10^{-4}	0.67459	—
4×10^{-4}	0.65719	0.0174
2×10^{-4}	0.64399	0.0132
1×10^{-4}	0.63660	0.0074
5×10^{-5}	0.63359	0.0030

TABLE 1. The angle of the wedge (in radians) for a decreasing set of surface tensions. The variation (third column) is the difference between consecutive angles, corresponding to surface tensions S and $2S$.

is more reasonable to compare the interfaces when their finger tips reach the same level above the sink. As surface tension is reduced, the finger tip reaches the given level faster. Figure 8 provides some indication of the asymptotic trend of the fingers as surface tension is successively halved from $S = 8 \times 10^{-4}$ to $S = 5 \times 10^{-5}$. We choose the fixed level to be $y = 0.01$ which is very close to the sink. Table 1 shows that the difference between consecutive angles (corresponding to surface tensions S and $2S$) decreases as surface tension is reduced. This strongly suggests that an asymptotic angle is selected for the wedge as it touches the sink.

But, what is the limiting behavior of the interface in the vicinity of the neck? Clearly, a potential neck singularity can only develop past t_c , the singularity time of the zero-surface-tension solution. Before t_c , we find that the small surface tension solution converges strongly to the zero-surface-tension solution. The interesting

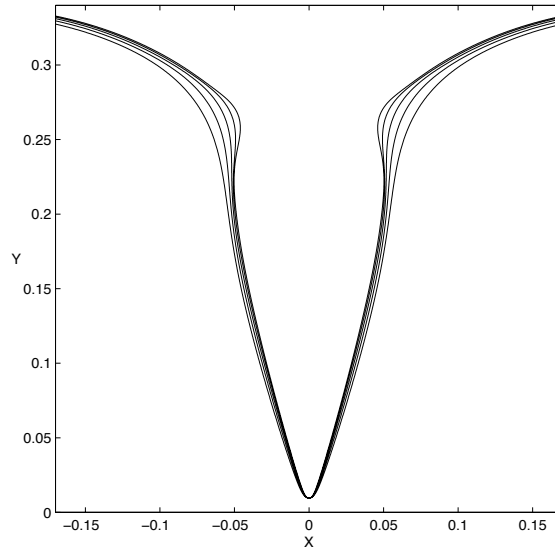


FIGURE 8. Comparison of the interface finger for a sequence of surface tensions. From the outer curve inwards, the fingers correspond to the surface tension values $S = 8 \times 10^{-4}$, 4×10^{-4} , 2×10^{-4} , 1×10^{-4} , and 5×10^{-5} . Each interface is plotted when the tip of the finger reaches the fixed level $y = 0.01$ at $x = 0$. $N = 16384$ and $\Delta t = 2 \times 10^{-7}$.

question is whether the small surface tension solution forms a neck singularity past t_c but before the time at which the limiting wedge reaches the sink. We find strong evidence that the small surface tension solution indeed forms a neck (corner) singularity in the limit as surface tension tends to zero. A pronounced neck with two corners can be clearly observed for $S = 5 \times 10^{-6}$ in Figure 9. A close inspection of its tangent angle and curvature also suggests formation of two corner singularities at the neck. Unfortunately, well-resolved computations for surface tensions smaller than this value become extremely difficult due to interface singular behavior and to growth of the round-off error noise.

The above numerical results provide us with a new understanding of the limiting behavior of small surface tension Hele-Shaw flow with suction. The two necking singularities past t_c are surprising in a sense. They seem to be responsible for the selection of limiting wedge angle. The fact that there is a well-defined limiting wedge angle defies our intuition (one may think that the wedge angle should decrease with surface tension). This also contradicts the assumption of the crack model in which a self-similar profile of the finger is assumed. In [CHS99], we also investigate the limiting behavior for two-phase Hele-Shaw flows, i.e. $A_\mu < 1$. We find that larger viscosity in the exterior fluid prevents the formation of the neck and leads to the development of thinner fingers. It is observed that the asymptotic wedge angle of the fingers decreases as the viscosity ratio is reduced, apparently towards the zero angle (cusp) of the zero-viscosity-ratio solution. For more discussions, we refer the reader to [CHS99]. It is natural to ask how the behavior of the interface would

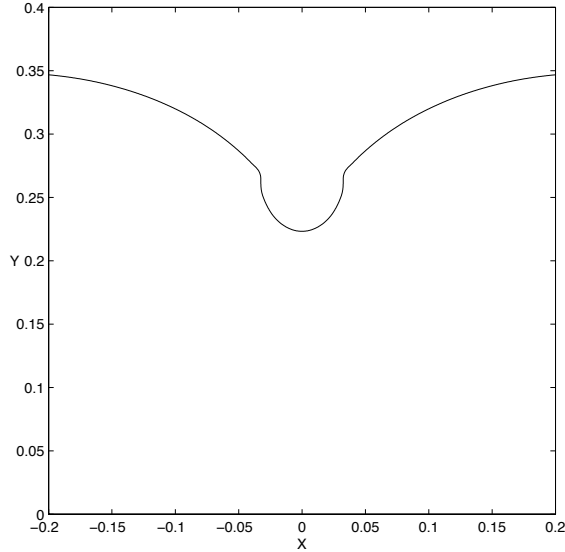


FIGURE 9. Close-up of the interface around $x = 0$ at $t = 0.2857$ (just past t_c) for $S = 5 \times 10^{-6}$. $N = 8192$ and $\Delta t = 5 \times 10^{-6}$.

be in the corresponding 3-D Darcy flow. Ceniceros and Si [CS99] address this problem numerically and find with surprise that the azimuthal component of the surface tension does not play an important role in this case. The limiting behavior is very similar to the 2-D flow studied here and no pinching singularity is found. This is in contrast with 3-D liquid jets. It is conceivable that the suction force plays a more dominant role than the azimuthal component of surface tension in this case.

5.4. Finger selection and noise effects in Hele-Shaw cells. Morphological instabilities are common to pattern formation problems. The non-equilibrium growth of crystals and directional solidification are some of the best known examples. Due to the underlying Mullins-Sekerka instability, very small perturbations caused by noise originate convoluted interfacial patterns when surface tension is small. The generic mechanisms in the formation of these complex patterns are present in the simpler problem of a Hele-Shaw interface. The purpose of this study is to investigate the impact of small surface tension on the pattern formation and selection of fingers.

We first formulate the Hele-Shaw problem in a way which is convenient for analysis. We rely on the conformal mapping technique on which most analyses are based. To this end, we represent the interface motion by a time-dependent conformal map $z(\zeta, t)$ that takes the interior of the unit circle in the ζ -plane onto the physical domain of the viscous fluid in the z -plane. The unit circle itself is mapped to the Hele-Shaw interface. Because of the presence of the source at the origin, z has the following form

$$(5.3) \quad z(\zeta, t) = \frac{a(t)}{\zeta} + f(\zeta, t),$$

where f is an analytic function inside the disk, and $a(t)$ is real and positive. We nondimensionalize all variables by taking the pumping rate $Q = 2\pi$ and $a(0) = 1$. Letting $Z(\alpha, t) = z(e^{i\alpha}, t)$, we obtain the following evolution equation (for a derivation see for example [CK91])

$$(5.4) \quad Z_t = F(Z_\alpha) + SG(Z_\alpha),$$

where

$$(5.5) \quad F(Z_\alpha) = -iZ_\alpha(I - iH)|Z_\alpha|^{-2},$$

and

$$(5.6) \quad G(Z_\alpha) = iZ_\alpha(I - iH)[|Z_\alpha|^{-2}H\mathcal{K}_\alpha].$$

Here \mathcal{K} is the mean curvature. The subscript α means differentiation with respect to that variable. H is the periodic Hilbert transform defined as

$$(5.7) \quad Hf(\alpha) = \frac{1}{2\pi} \int_0^{2\pi} \cot \frac{1}{2}(\alpha - \alpha') f(\alpha') d\alpha'.$$

Many exact solutions have been found for the zero surface tension problem (see, e.g. [Saf59, How86a, How86b, How86c, SB84]). Here we are interested in comparing non-zero S solutions with those zero-surface-tension solutions for which $z_\zeta(\zeta, 0)$ has at least one zero in the extended complex domain $|\zeta| > 1$. For concreteness, we consider the following expanding bubble with three-fold symmetry:

$$(5.8) \quad z(\zeta, t) = \frac{A(t)}{\zeta} \left[1 + \frac{\zeta^3}{2\zeta_0^3(t)} \right],$$

where $A(t)$ and $\zeta_0(t)$ have analytical expressions (see [SB84]). The parameters $A(0)$ and $\zeta_0(0)$ are real numbers satisfying $A(0) > 0$ and $|\zeta_0(0)| > 1$. The derivative z_ζ has three zeros in $|\zeta| > 1$ which approach the unit disk and impinge on it at a time t_c . This particular set of initial data has been used by Siegel, Tanveer, and Dai [STD96]. In our study, we choose $A(0) = 1$ and $\zeta_0(0) = 1.2$. With this choice of initial data, $t_c = 0.3301$. At t_c , the zero-surface-tension solution forms three cusp singularities.

5.4.1. The daughter singularity. Before we proceed to our numerical study, we need to describe briefly the perturbation analysis of Tanveer [Tan93] and Siegel, Tanveer, and Dai [STD96]. The perturbation analysis requires to extend the equations of motion to $|\zeta| > 1$. First, equation (5.4) can be analytically continued into the domain $|\zeta| < 1$ by the use of Poisson integral formula. The analytic continuation to $|\zeta| > 1$ is achieved by contour deformation.

In the domain $|\zeta| > 1$, the extended evolution equation has the following form

$$(5.9) \quad z_t = q_1 z_\zeta + q_2 + S(q_3(z_\zeta)_{\zeta\zeta}^{-1/2} + r),$$

where q_1 , q_2 , and q_3 are analytic functions of ζ in $|\zeta| > 1$. The term $(z_\zeta)_{\zeta\zeta}^{-1/2}$ contains the leading order contribution from surface tension. The function r contains those surface tension terms which are less singular than $(z_\zeta)_{\zeta\zeta}^{-1/2}$ in the neighborhood of a zero of $z_\zeta(\zeta, 0)$. We do not write the explicit forms of these functions since they play no role in the leading order asymptotic analysis.

When performing a perturbation analysis, it is important to choose a function space and an associated norm so that the limiting problem is well-posed in this function space. Although the zero-surface-tension problem is ill-posed in the physical space, it becomes well-posed in the extended complex domain. Thus, it makes

sense to perform a perturbation expansion in the extended $|\zeta| > 1$ domain for small S :

$$(5.10) \quad z(\zeta, t) = z_0(\zeta, t) + Sz_1(\zeta, t) + \dots,$$

where z_0 is the zero-surface-tension solution [Tan93]. It is easy to see that z_0 and z_1 satisfy the following equations:

$$(5.11) \quad z_{0t} = q_{10}z_{0\zeta} + q_{20}$$

$$(5.12) \quad z_{1t} = q_{10}z_{1\zeta} + q_{30}(z_{0\zeta})_{\zeta\zeta}^{-1/2} + \dots,$$

where the subscript 0 on any q_i term denotes its evaluation using the corresponding $S = 0$ solution.

It is worth noting that the leading order surface tension term enters the z_1 equation as a known forcing function. This singular forcing function contains a branch point singularity when $z_{0\zeta} = 0$ in $|\zeta| > 1$. Thus, if the initially given z has a zero in z_ζ in the extended $|\zeta| > 1$ domain, i.e.

$$(5.13) \quad z_\zeta(\zeta, 0) \sim D(0)(\zeta - \zeta_0(0)) \quad \text{for } |\zeta_0(0)| > 1,$$

then the singular forcing term $(z_{0\zeta})_{\zeta\zeta}^{-1/2}$ will generate a new complex singularity at $t = 0^+$ at $\zeta = \zeta_0(0)$. The solution for z_1 will have the form

$$(5.14) \quad z_1 \sim A_0(t)(\zeta - \zeta_0(t))^{-3/2} + A_d(t)(\zeta - \zeta_d(t))^{-3/2}$$

with $A_0(0) + A_d(0) = 0$. The spawn daughter singularity $\zeta_d(t)$ moves according to the following equation

$$(5.15) \quad \dot{\zeta}_d(t) = -q_{10}(\zeta_d(t), t) \quad \text{with } \zeta_d(0) = \zeta_0(0),$$

whereas the motion of the zero $\zeta_0(t)$ is governed by

$$(5.16) \quad \dot{\zeta}_0(t) = -q_{10}(\zeta_0(t), t) - q_{20\zeta}(\zeta_0(t), t)[z_{\zeta\zeta}(\zeta_0(t), t)]^{-1}.$$

Thus, $\zeta_0(t)$ and $\zeta_d(t)$ travel at very different speeds. Depending on the initial data, it is possible that $\zeta_d(t)$ could reach the unit disk first when the zero is still far from it. For future reference, we define t_d to be the time at which the solution to (5.15) reaches the unit disk. For the data we consider here, we can solve the above ODE numerically to obtain $t_d = 0.0463$, which is much smaller than $t_c = 0.3301$. At t_d , ζ_d reaches the unit disk and the daughter singularity becomes a physical singularity for z_1 . According to the prediction of Tanveer and Siegel, Tanveer, and Dai, the nonzero surface tension solution can deviate significantly from the corresponding zero-surface-tension solution no matter how small the surface tension is, even though the zero-surface-tension solution is still analytic at t_d . Further inner asymptotic analysis of [Tan93] suggests that the initial singularity $\zeta_d(0)$ is transformed by the presence of surface tension into cluster of an infinite number of $-4/3$ singularities. The cluster is localized around $\zeta_d(t)$ before it breaks up and disperse near the unit disk.

5.4.2. An effective numerical method to study the limit. The daughter singularity theory is quite surprising and is a bit counter intuitive at first glance. Numerical results in [STD96] give partial confirmation of this singular perturbation of small surface tension to Hele-Shaw flows. But due to the extreme noise sensitivity, Siegel, Tanveer, and Dai find it very difficult to compute for $S < 10^{-5}$, even if quadruple (128-bit) precision was used.

In [CH00], we develop a novel numerical method to overcome the difficulties mentioned above. Our method relies on three key observations. The first one is that noise can be significantly reduced by using a parametrization that yields a compact representation of the solution in Fourier space. Out of many choices (Lagrangian, equal-arclength, etc.), we find that the conformal map representation gives the most compact parametrization of the interface. This compact parametrization has also been used by Dai and Shelley [DS93] and by Siegel, Tanveer, and Dai [STD96]. With this parametrization, we can use effectively Krasny filtering [Kra86] to separate noise from the physical solution for the majority of high to intermediate modes. Moreover, we can also perform selective filtering based on the symmetry of the solution.

The second observation is to derive a scaled equation for the leading order perturbation. The reason for doing this is because the daughter singularity is only born at $t = 0^+$. For times of $O(\Delta t)$, the amplitude of the daughter singularity is $O(S\Delta t)$. Moreover, since the daughter singularity is still far from the unit disk, the interface is analytic and its Fourier modes decay exponentially, in a rate of $\frac{S\Delta t}{|\zeta_d|^k}$, where k is the wave number. Therefore, many digits are required to capture the presence of the singularity in the complex plane.

In order to effectively capture the complex singularity, we need to factor out the small surface tension coefficient in front of the complex singularity. One way to do this is to derive a scaled equation for the perturbed quantity. Specifically, we obtain an evolution equation for the scaled deviation, $\tilde{Z} = (Z - Z_0)/S$, where Z_0 is the known zero-surface-tension solution. Note that Z_0 satisfies the equation $Z_{0t} = F(Z_{0\alpha})$. Subtracting this equation from (5.4) we get

$$(5.17) \quad \tilde{Z}_t = \frac{1}{S}[F(Z_{0\alpha} + S\tilde{Z}_\alpha) - F(Z_{0\alpha})] + G(Z_{0\alpha} + S\tilde{Z}_\alpha),$$

which can be further simplified to ¹

$$(5.18) \quad \tilde{Z}_t = iZ_\alpha(I - iH)h(\alpha) + i\tilde{Z}_\alpha(I - iH)|Z_{0\alpha}|^{-2} + G(Z_{0\alpha} + S\tilde{Z}_\alpha),$$

where

$$(5.19) \quad h(\alpha) = \frac{2\text{Re}(\tilde{Z}_\alpha/Z_{0\alpha}) + S|\tilde{Z}_\alpha/Z_{0\alpha}|^2}{|Z_\alpha|^2}.$$

Thus, the small surface tension coefficient is factored out from the scaled equation completely.

Our third observation is that we need to perform a resolution study in the precision digits and the filter level. To achieve this, we use very *high precision arithmetic* to solve numerically the scaled equation (5.17). High precision has the additional benefit of reducing the amplitude of the round-off noise. Variable high precision (up to 80 digits) was accomplished in this work with the use of the multi-precision package developed by Bailey [Bai90]. All these three ingredients are essential in capturing the singular behavior of the small surface tension solution.

5.4.3. *Numerical results.* We first present our computations performed for $S = 10^{-7}$, 10^{-8} , and 10^{-9} (the computations presented here actually used the original \tilde{Z} equation presented in [CH00]). In our numerical computations, we start with $N = 4096$. N is doubled to 8196 when the magnitude of the highest Fourier mode exceeded the filter level. The time-step is then reduced by a factor of 8.

¹This improved formula was pointed out to us by an anonymous referee.

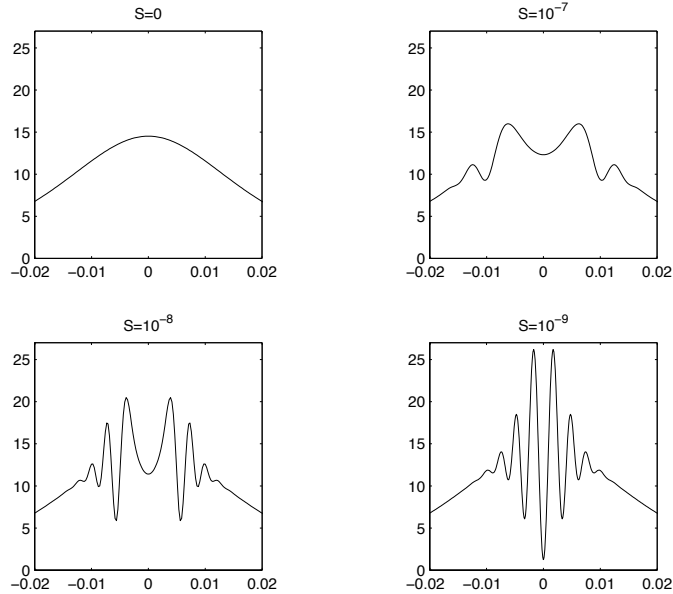
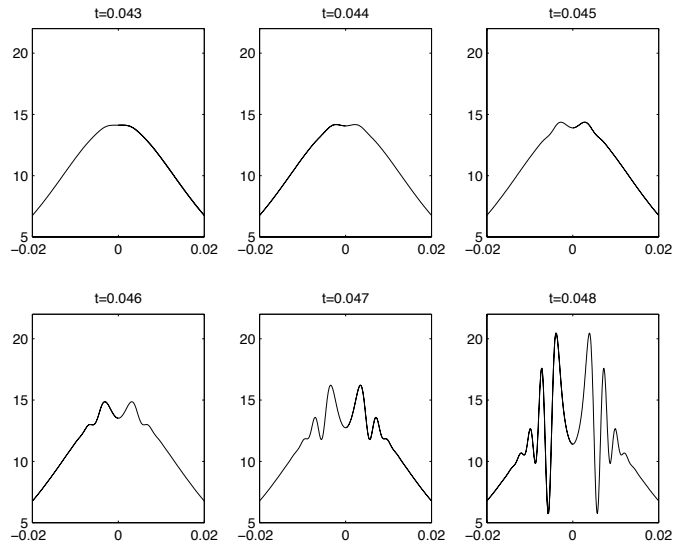
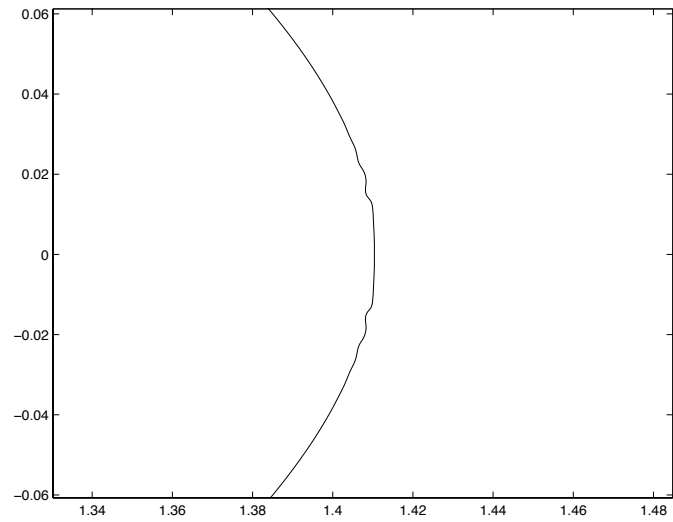


FIGURE 10. Curvature vs $\alpha/2\pi$ around one tip of the interface at $t = 0.048$ for $S = 0, 10^{-7}, 10^{-8}$, and 10^{-9} . $N = 8192$. Precision level 60 . Filter level 10^{-56} .

We use the 60-digit computations for all the values of S which are found to be in good agreement with the 80-digit computations. The singular nature of the asymptotic solution can be seen clearly in the deviations of the $S > 0$ curvatures from the corresponding zero-surface-tension curvature. As observed in Figure 10, the deviations are significant and rather localized at the fixed time $t = 0.048$. Indeed, the smaller the surface tension the larger the deviation.

Next, we present first a sequence of pictures of the interface curvature near one tip at early times near t_d (Figure 11), now for a fixed surface tension. The computations correspond to $S = 10^{-8}$. One can already feel the effect of the daughter singularity in the physical domain at the time $t = 0.043$ around the interface tips. At $t = 0.043$, the tip curvature flattens in a very localized finite region. This is in agreement with the theoretical estimate of the daughter singularity impact time. After $t = 0.046$ on, the curvature develops large deviations from the zero-surface-tension curvature. The affected physical regions near the three tips also spread in time. This behavior is consistent with the asymptotic theory which implies that daughter singularity cluster will disperse once it gets sufficiently close to the unit disk. It is worth pointing out that the length scale decreases in time while the amplitude grows in time. During this process, the impact of the daughter singularity on the physical domain becomes more pronounced.

We would like to perform a long time calculation to identify the impact of the daughter singularity on the interface. To do this, we first compute up to t_d using 60-digit arithmetic. Shortly after that, we switch to double precision when the highest mode of \tilde{Z} is about 10^{-15} . The number of points is doubled whenever the spectrum becomes under-resolved. Finally we stop the computation with $N =$


 FIGURE 11. Tip curvature for $S = 10^{-8}$ at early times near $t_d = 0.0463$.

 FIGURE 12. Close-up of the interface at $t = 0.0502$ for $S = 10^{-8}$.

32768 and $\Delta t = 10^{-7}$. In this calculation, we find that the curvature grows rapidly at subsequent times. In a very short time interval, the maximum of curvature has grown more than 10 times its value at $t = 0.049$, and the singular regions continue to spread in time. In Figure 12, we can see that the singular effects are already visible in the interface. The small indentations near the interface tip correspond to the largest curvature transition. These side indentations are a signature of surface tension.

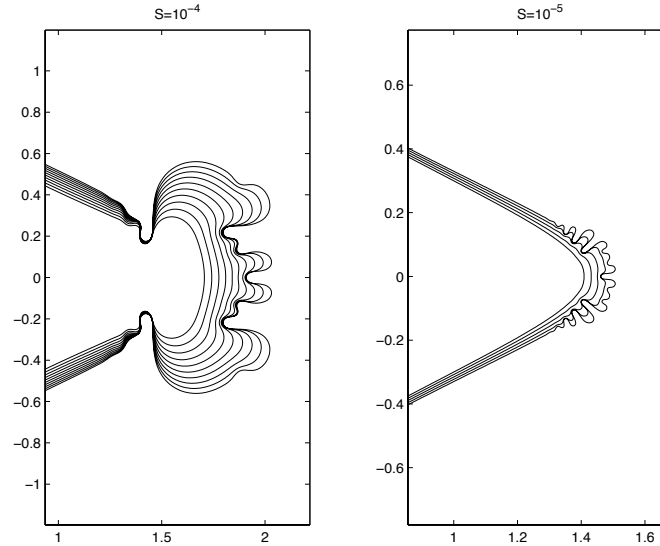


FIGURE 13. Close-ups of the Hele-Shaw interface at different times for $S = 10^{-4}$ ($t = 0.23-0.50$, with a 0.03 time difference between profiles) and $S = 10^{-5}$ ($t = 0.05-0.09$, with a 0.01 time difference between profiles). Computation performed with the equal-arclength method.

To better illustrate the impact of daughter singularity on the physical domain, we present two more computations with larger surface tensions using the the equal-arclength method of HLS [HLS94]. The method presented in this subsection cannot compute accurately for larger surface tension due to severe time-stepping limitations. Figure 13 shows the close-up of the evolution of the interface near one tip for $S = 10^{-4}$ and $S = 10^{-5}$ respectively. The symmetric indentations are clearly formed before the noise-induced tip splitting occurs. For $S = 10^{-5}$, the side indentations produced by surface tension begin to be visible in the second curve from left to right. Shortly after that the tip-splitting process and the finger formation begin. The above calculations also suggest that surface tension defines a length scale of the finger width. According to the asymptotic theory, this length scale is related to the minimum distance of the complex singularity to the unit disk.

References

- [Bai90] D. H. Bailey, *MPFUN: A portable high performance multiprecision package*, Tech. Report RNR-90-022, NASA Ames Research Center, 1990.
- [Bea98] J. T. Beale, *A convergent boundary integral method for 3-D water waves*, preprint, submitted to Math. Comput., 1998.
- [BHL96] J. T. Beale, T. Y. Hou, and J. S. Lowengrub, *Convergence of a boundary integral method for water waves*, SIAM J. Numer. Anal. **33** (1996), no. 5, 1797–1843.
- [BMO80] G. R. Baker, D. I. Meiron, and S. A. Orszag, *Vortex simulations of the Rayleigh-Taylor instability*, Phys. Fluids **23** (1980), 1485–1490.
- [BMO82] G. R. Baker, D. I. Meiron, and S. A. Orszag, *Generalized vortex methods for free-surface flow problems*, J. Fluid Mech. **123** (1982), 477–501.
- [CH98] H. D. Ceniceros and T. Y. Hou, *Convergence of a non-stiff boundary integral method for interfacial flows with surface tension*, Math. Comput. **67** (1998), 137–182.

- [CH99] H. D. Cenicerros and T. Y. Hou, *Dynamic generation of capillary waves*, Phys. Fluids **11** (1999), no. 5, 1042–1050.
- [CH00] H. D. Cenicerros and T. Y. Hou, *The singular perturbation of surface tension in Hele-Shaw flows*, J. Fluid Mech. **409** (2000), 251–272.
- [CHS99] H. D. Cenicerros, T. Y. Hou, and H. Si, *Numerical study of Hele-Shaw flow with suction*, Phys. Fluids **11** (1999), no. 9, 2471–2486.
- [CK91] P. Constantin and L. Kadanoff, *Dynamics of a complex interface*, Physica D **47** (1991), 450–460.
- [CP93] P. Constantin and M. Pugh, *Global solutions for small data to the Hele-Shaw problem*, Nonlinearity **6** (1993), 393–415.
- [Cra70] G. D. Crapper, *Non-linear capillary waves generated by steep gravity waves*, J. Fluid Mech. **40** (1970), 149–159.
- [CS99] H. D. Cenicerros and H. Si, *Computation of axi-symmetric suction flow through porous media in the presence of surface tension*, preprint, submitted to J. Comput. Phys., 1999.
- [Dol92] J. W. Dold, *An efficient surface-integral algorithm applied to unsteady gravity waves*, J. Comput. Phys. **103** (1992), 90–115.
- [DQPW99] J. H. Duncan, H. Qiao, V. Philomin, and A. Wenz, *Gentle spilling breakers: crest profile evolution*, J. Fluid Mech. **379** (1999), 191–222.
- [DR81] P. G. Drazin and W. H. Reid, *Hydrodynamic stability*, Cambridge monographs on mechanics and applied mathematics, Cambridge University Press, New York, 1981.
- [DR84] J. Duchon and R. Robert, *Évolution d’une interface par capillarité et diffusion de volume I. Existence locale en temps*, Ann. Inst. Henri Poincaré **1** (1984), no. 5, 361–378.
- [DS93] W.-S. Dai and M. J. Shelley, *A numerical study of the effect of surface tension and noise on an expanding Hele-Shaw bubble*, Phys. Fluids A **5** (1993), no. 9, 2131–2146.
- [EKT87] N. Ebuchi, H. Kawamura, and Y. Toba, *Fine structure of laboratory wind-waves surfaces studied using an optical method*, Boundary Layer Met. **39** (1987), 133–151.
- [HKS98] T. Y. Hou, I. Klapper, and H. Si, *Removing the stiffness of curvature in computing 3-D filaments*, J. Comput. Phys. **143** (1998), 628–664.
- [HLO88] S. D. Howison, A. A. Lacey, and J. R. Ockendon, *Hele-Shaw free-boundary problems with suction*, Q. JI Mech. Appl. Math. **41** (1988), 183–193.
- [HLS94] T. Y. Hou, J. S. Lowengrub, and M. J. Shelley, *Removing the stiffness from interfacial flows with surface tension*, J. Comput. Phys. **114** (1994), 312–338.
- [HLS97] T. Y. Hou, J. S. Lowengrub, and M. J. Shelley, *The long-time motion of vortex sheets with surface tension*, Phys. Fluids **9** (1997), no. 7, 1933–1954.
- [How86a] S. D. Howison, *Bubble growth in porous media and Hele-Shaw cells*, Proc. R. Soc. Edinb. A **102** (1986), 141–148.
- [How86b] S. D. Howison, *Cusp development in Hele-Shaw flow with a free surface*, SIAM J. Appl. Math. **46** (1986), 20–26.
- [How86c] S. D. Howison, *Fingering in Hele-Shaw cells*, J. Fluid Mech. **167** (1986), 439–435.
- [HZa] T. Y. Hou and P. Zhang, *A new stabilizing technique for boundary integral methods*, Math. Comput., to appear.
- [HZb] T. Y. Hou and P. Zhang, *Stability of a boundary integral method for 3-D water waves*, preprint, submitted to SIAM J. Numer. Anal.
- [KH97] E. D. Kelly and E. J. Hinch, *Numerical simulations of sink flow in the Hele-Shaw cell with small surface tension*, Euro. Jnl. of Applied Maths **8(6)** (1997), 533–550.
- [Kra86] R. Krasny, *A study of singularity formation in a vortex sheet by the point vortex approximation*, J. Fluid Mech. **167** (1986), 65–93.
- [LH95] M. S. Longuet-Higgins, *Parasitic capillary waves: a direct calculation*, J. Fluid Mech. **301** (1995), 79–107.
- [LH96] M. S. Longuet-Higgins, *Capillary jumps on deep water*, Journal of Physical Oceanography **26** (1996), 1957–1965.
- [LHC76] M. S. Longuet-Higgins and E. D. Cokelet, *The deformation of steep surface waves on water I. A numerical method of computation*, Proc. R. Soc. Lond. A. **350** (1976), 1–26.
- [NT98] Q. Nie and F. R. Tian, *Singularities in Hele-Shaw flows*, SIAM J. Appl. Math **58(1)** (1998), 34–54.

- [Pat81] L. Paterson, *Radial fingering in a Hele-Shaw cell*, J. Fluid Mech. **113** (1981), 513–529.
- [Pel88] P. Pelcé, *Dynamics of curved fronts*, Academic Press, Inc., San Diego, 1988.
- [PLT93] M. Perlin, H. Lin, and C.-L. Ting, *On parasitic capillary waves generated by steep gravity waves: an experimental investigation with spatial and temporal measurements*, J. Fluid Mech. **255** (1993), 597–620.
- [Pul82] D. I. Pullin, *Numerical studies of surface-tension effects in nonlinear Kelvin-Helmholtz and Rayleigh-Taylor instability*, J. Fluid Mech. **119** (1982), 507–532.
- [Ric72] S. Richardson, *Hele-Shaw flows with a free boundary produced by the injection of fluid into a narrow channel.*, J. Fluid Mech. **56** (1972), 609–618.
- [Rob83] A. J. Roberts, *A stable and accurate numerical method to calculate the motion of a sharp interface between fluids*, IMA J. Appl. Math. **31** (1983), 13–35.
- [Ros32] L. Rosenhead, *The point vortex approximation of a vortex sheet*, Proc. Roy. Soc. London Ser. A **134** (1932), 170–192.
- [RS88] R.H. Rangel and W.A. Sirignano, *Nonlinear growth of Kelvin-Helmholtz instability: Effect of surface tension and density ratio*, Phys. Fluids **31** (1988), no. 7, 1845–1855.
- [Saf59] P. G. Saffman, *Exact solutions for the growth of fingers from a flat interface between two fluids in a porous medium*, Q. J. Mech. Appl. Maths **12** (1959), 146–150.
- [SB84] B. Shraiman and D. Bensimon, *Singularities in nonlocal interface dynamics*, Phys. Rev. A. **30** (1984), no. 5, 2840–2842.
- [She92] M. J. Shelley, *A study of singularity formation in vortex sheet motion by a spectrally accurate vortex method*, J. Fluid Mech. **244** (1992), 493–526.
- [ST58] P. G. Saffman and G. I. Taylor, *The penetration of fluid into a porous medium or Hele-Shaw cell*, Proc. Roy. Soc. A. **245** (1958), 312–329.
- [STD96] M. Siegel, S. Tanveer, and W.-S. Dai, *Singular effects of surface tension in evolving Hele-Shaw flows*, J. Fluid Mech. **323** (1996), 201–236.
- [TA83] G. Tryggvason and H. Aref, *Numerical experiments in Hele-Shaw flows with a sharp interface*, J. Fluid Mech. **136** (1983), 1–30.
- [Tan93] S. Tanveer, *Evolution of Hele-Shaw interface for small surface tension*, Phil. Trans. R. Soc. Lond. A **343** (1993), 155–204.
- [Tia95] F.R. Tian, *On the breakdown of Hele-Shaw solutions with non-zero surface tension*, J. Nonlinear Sci. **5** (1995), 479–484.
- [Tul96] M. P. Tulin, *Breaking of ocean waves and downshifting*, Waves and Nonlinear Processes in Hydrodynamics, Kluwer Academic Publishers, 1996, pp. 177–190.
- [Wu97] S. J. Wu, *Well-posedness in Sobolev spaces of the full water wave problem in 2-D*, Invent. Math. **130** (1997), 39–72.

APPLIED MATHEMATICS, CALIFORNIA INSTITUTE OF TECHNOLOGY, PASADENA, CA 91125
E-mail address: `hdc@ama.caltech.edu`

APPLIED MATHEMATICS, CALIFORNIA INSTITUTE OF TECHNOLOGY, PASADENA, CA 91125
E-mail address: `hou@ama.caltech.edu`